Eur. J. Biochem. **269**, 4879–4886 (2002) © FEBS 2002 doi:10.1046/j.1432-1033.2002.03193.x

Proximal ligand motions in H93G myoglobin

Stefan Franzen[1], Eric S. Peterson[2], Derek Brown[1], Joel M. Friedman[3], Melissa R. Thomas[4] and Steven G. Boxer[4]

[1]*Department of Chemistry, North Carolina State University, Raleigh, NC, USA;* [2]*Chemistry Department, Bowdoin College, 6600 College Station, Brunswick, ME 04011-8466, USA;* [3]*Department of Physiology and Biophysics, Albert Einstein College of Medicine, Bronx, NY, USA;* [4]*Department of Chemistry, Stanford University, Stanford, CA, USA*

Resonance Raman spectroscopy has been used to observe changes in the iron–ligand stretching frequency in photoproduct spectra of the proximal cavity mutant of myoglobin H93G. The measurements compare the deoxy ferrous state of the heme iron in H93G(L), where L is an exogenous imidazole ligand bound in the proximal cavity, to the photolyzed intermediate of H93G(L)*CO at 8 ns. There are significant differences in the frequencies of the iron–ligand axial out-of-plane mode ν(Fe–L) in the photoproduct spectra depending on the nature of L for a series of methyl-substituted imidazoles. Further comparison was made with the proximal cavity mutant of myoglobin in the absence of exogenous ligand (H93G) and the photoproduct of the carbonmonoxy adduct of H93G (H93G-*CO). For this case, it has been shown that H_2O is the axial (fifth) ligand to the heme iron in the deoxy form of H93G. The photoproduct of H93G-*CO is consistent with a transiently bound ligand proposed to be a histidine. The data presented here further substantiate the conclusion that a conformationally driven ligand switch exists in photolyzed H93G-*CO. The results suggest that ligand conformational changes in response to dynamic motions of the globin on the nanosecond and longer time scales are a general feature of the H93G proximal cavity mutant.

Keywords: resonance Raman, heme, myoglobin, hemoglobin, ligand switch.

Protein structural relaxation following heme photolysis has been studied in globins as a means to obtain information on structural intermediates following diatomic ligand photolysis. In hemoglobin (Hb), time-resolved spectroscopic studies have provided information on the time scale for transition from the six-coordinate R state to the five-coordinate T-state [1–3]. The proximal cavity mutant of Hb has recently demonstrated the key role of the proximal histidine in the cooperativity of quaternary structure change in response to ligand binding [4]. Strain in the covalent bond to the heme iron of Hb can be monitored by following the shift in frequency of the iron–histidine axial mode, ν(Fe–His), by time-resolved resonance Raman spectroscopy [5]. In myoglobin (Mb), these studies have indicated a much smaller change in structure [6]: the observed frequency shift of the iron–histidine band is *c.* 1.6 cm^{-1} on the 8 ns time scale compared to 12 cm^{-1} in Hb. Nonetheless, this shift in the ν(Fe–His) Raman band is significant because shifts in absorption bands (the time-dependent Soret band shift and band III shift) have been attributed to iron out-of-plane displacement that should also be coupled to ν(Fe–His) [7–10]. A structural interpretation of these observable phenomena helps to bridge the gap between the extensive X-ray crystallography studies and the thermodynamic and kinetic data available for Mb [7,11–20].

Histidine-ligated heme enzymes have a surprisingly large range of functions. In peroxidase, a charge relay due to hydrogen bonding of the imidazole ring of histidine permits the formation of high valent iron oxidation states that play a role in the redox function of these enzymes [21–23]. Charge relay effects are seen in other heme proteins such as the transcriptional activator CooA [24]. Enhanced enzyme activity is triggered by the rupture of the histidine-iron bond in guanylyl cyclase in response to *trans* NO ligation [25,26], None of these effects are as clearly observed in wild-type Mb, although recent work suggests that Mb does in fact play an enzymatic role in catalyzing reactions of small molecules such as O_2, CO, NO and peroxides [27]. Presumably, the imidazole ring is appropriately stabilized in the proximal pocket of Mb by hydrogen bonding and steric effects. The hydrogen bonding of the proximal iron ligand, His93 in Mb is thought to be relatively weak. The Nδ proton has a bifurcated hydrogen bonding interaction with the lone pair of the Ser92 hydroxyl and the backbone carbonyl of Leu89 [11,28]. The role of hydrogen bonding can be addressed by studies of the Mb proximal cavity mutant (H93G) for a series of axial proximal ligands in addition to mutants such as S92A that change the hydrogen bonding environment of the proximal pocket [29]. Studies of the H93G mutant with a series of different ligands in the proximal cavity have the advantage of probing proximal effects on both proximal ligand rebinding and stability as well as how these couple to the distal pocket where small diatomic ligands, such as CO, bind [30].

This study investigates the dynamics that occur within the first 8 ns following photolysis of CO in the H93G mutant with four different imidazole ligands in the proximal cavity.

Correspondence to Stefan Franzen, Department of Chemistry, North Carolina State University, Raleigh, NC 27695, USA.
Fax: +1 919 515 8909, Tel.: + 1 919 515 8915,
E-mail: Stefan_Franzen@ncsu.edu

Abbreviations: Hb, hemoglobin; Im, imidazole; x-MeIm, x-methyl imidazole (x = 1, 2 or 4); Mb, myoglobin.

(Received 3 December 2001, revised 17 July 2002, accepted 20 August 2002)

The H93G mutant permits substitution of different organic ligands to the heme iron by simple dialysis [31]. The ligands studied here are imidazole (Im), 1-methyl imidazole (1-MeIm), 2-methyl imidazole (2-MeIm) and 4-methyl imidazole (4-MeIm). Additionally, data are presented for the proximal cavity mutant in the absence of exogenous ligand (H93G). In this case the axial ligand *trans* to CO is one of the histidine residues located in the heme pocket of the globin [32]. Experimental comparison of the deoxy form for a ligand L [denoted H93G(L)] and the photolyzed CO form [denoted H93G(L)*CO] permits a comparison of the equilibrium deoxy state with that of a nonequilibrium state very close to that of the ligated species. The photoproduct and deoxy states are both five-coordinate. However, in the photoproduct, the frequency of the iron-ligand axial vibrational mode observed during the first 8 ns following photolysis is typically shifted to higher frequencies due to a nonequilibrium protein conformation surrounding the heme in which the covalent bond between the heme iron and the proximal ligand is experiencing less strain. Thus, the photoproduct spectra of the H93G(L) series are snapshots on the 8 ns time scale that provide a measure of the varying degrees of strain on the proximal ligand that can be compared with Mb protein structures and CO rebinding kinetics [30]. This comparison is important because proximal strain is typically hypothesized to be a major component in the rebinding barrier to the CO ligand. The data obtained here pertain to the effects of conformational strain when non-native imidazole ligands are bound to the heme iron and thereby give some information as to how crucial the particular geometry present in the wild-type protein is to its function. Finally, these data substantiate a model for a dynamic ligand switch in H93G Mb when no exogenous ligand is present.

EXPERIMENTAL PROCEDURES

The H93G mutants were obtained by applying cassette mutagenesis to the sperm whale Mb gene in the plasmid pMb413b as described previously [32]. The Mb proteins were expressed in *Escherichia coli* and purified in buffer containing 10 mM imidazole following standard procedures described previously [31]. Samples were prepared in 10 mM phosphate buffer at pH 7. The 8 ns photoproduct spectra were obtained by a one color resonance Raman experiment. The 435.8-nm (20 Hz, 8 ns pulses) excited resonance Raman spectra of both the 8 ns photoproduct of the CO-bound derivatives and the equilibrium five coordinate species were generated using a previously described apparatus [6,33].

RESULTS

The four panels of Fig. 1 show the peak assigned to the ν(Fe–L) stretching mode of the equilibrium H93G(L) deoxy and 8 ns H93G(L)*CO photoproduct resonance Raman spectra for the H93G adducts of four ligands to the heme iron in buffer solution. The peak frequencies for each species and the frequency difference between the photoproduct and the deoxy frequencies (*CO-deoxy) are given in Table 1. Again, although both spectra in each panel were obtained under identical excitation conditions, the deoxy H93G(L) five-coordinate species is at equilibrium, while the photolyzed carbonmonoxy species H93G(L)*CO is a transiently formed deoxy intermediate close to the ligated state. The ν(Fe–L) frequencies of the adducts H93G(Im), and H93G(4-MeIm) show a small shift of $-1\ cm^{-1}$ in the 8 ns photoproduct spectra relative to the equilibrium deoxy species. In wild-type Mb, the CO photoproduct frequency shift is of similar magnitude ($+1.5\ cm^{-1}$), but opposite direction as compared to the data for H93G(Im) and H93G(4-MeIm) (Peterson, E. & Friedman, J.M., unpublished results). It is noteworthy that the structure of H93G(4-MeIm) is the closest to that of the wild type in that the methyl group is attached to the imidazole ring at the same position as in wild-type histidine [34]. It is interesting the that band shape of ν(Fe–L) for H93G(4-MeIm) is also similar to wild type and that the shoulder at $240\ cm^{-1}$ that has been assigned as ν_9 is also present only with this exogenous ligand [35].

The 1-methyl imidazole adduct shown in Fig. 1(C) shows a bimodal peak. Isotope data for 1-methyl imidazole (1,3-^{15}N-substituted 1-MeIm) strongly suggest that this band is split by a Fermi resonance [36]. The deoxy and CO photoproduct spectra for H93G(1-MeIm) show two Fermi resonance bands that change significantly in intensity. However, a fit of the data to a sum of two Gaussian functions reveals essentially no shift. In contrast to the other proximal ligands studied in buffer solution, the 8 ns photoproduct spectrum of the H93G 2-methyl imidazole adduct has a ν(Fe–L) frequency that is $12\ cm^{-1}$ higher than

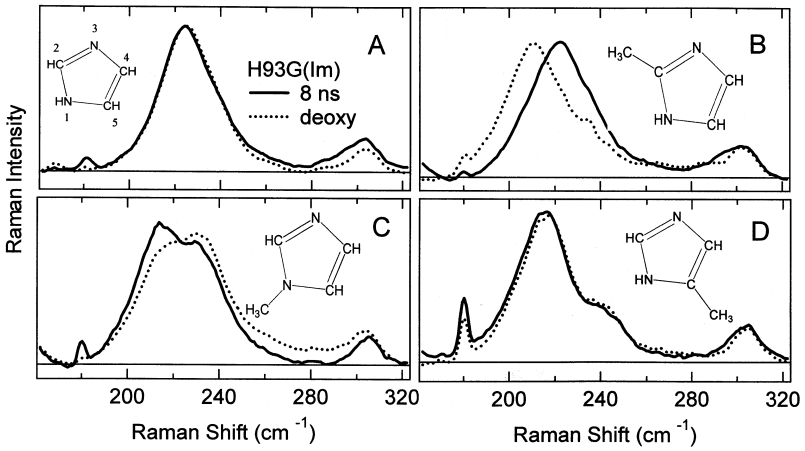

Fig. 1. Equilibrium deoxy and 8 ns CO photoproduct resonance Raman spectra for H93G(L) Mb with exogenous ligands in buffer solution. (A) L = imidazole; (B) L = 2-MeIm; (C) L = 1-MeIm; and (D) L = 4-MeIm. The proximal ligands are shown with the number scheme in each panel of the Figure. The feature at $180\ cm^{-1}$ is artifact from the hydrogen Raman shifter used in the experiment. The mode at $\approx 300\ cm^{-1}$ is γ_7 [35].

Table 1. Frequencies of ν(Fe–L) Raman modes for H93G(L) in buffer and 90% glycerol/buffer solutions. Frequencies of the Raman shift for the equilibrium deoxy and 8 ns CO photoproduct spectra are given for each adduct. All values are presented in cm^{-1}.

Species	Buffer deoxy	Buffer *CO	Difference (*CO-deoxy)	Glycerol deoxy	Glycerol *CO	Difference (*CO-deoxy)
H93G(Im)	225	224	−1	222	224	2
H93G(1-MeIm)	212 + 234	213 + 234	0	213 + 234	213 + 234	0
H93G(2-MeIm)	211	222	+11	213	221	+8
H93G(4-MeIm)	216	215	−1	212	216	+4
Wild type	218.4	219.7	1.3	216	220	+4

that of the equilibrium H93G(2-MeIm) deoxy species. This large shift in frequency is remarkably similar in magnitude and direction to that observed in the 8 ns photoproduct spectrum for wild-type human Hb [5].

The four panels of Fig. 2 show the equilibrium deoxy and 8 ns CO photoproduct spectra for the ν(Fe–L) band of H93G(Im), H93G(1-MeIm), H93G(2-MeIm), and H93G(4-MeIm) adducts in 90% glycerol/buffer solution. The ν(Fe–L) frequencies of both the equilibrium deoxy and the 8 ns photoproduct species are significantly dependent on the presence of glycerol. In the deoxy species no protein relaxation occurs, suggesting that glycerol affects the electrostatic environment of the heme. Increased osmotic pressure due to glycerol removes a distal water molecule, inducing a shift in ν(Fe–L) typically toward lower frequency. In contrast, the frequency shift in photoproduct spectra is ascribed to a slowing of the protein relaxation following photolysis, and thus the frequency is typically higher in a viscous solvent, such as glycerol, compared with buffer. A frequency shift of 2.6 cm^{-1} in the ν(Fe–His) band of the CO photoproduct for wild-type sperm whale Mb has been observed in 90% glycerol/buffer relative to buffer [37] and is in agreement with the data in Table 1. The imidazole and 4-methyl imidazole deoxy adducts show shifts of 3 and 4 cm^{-1}, respectively, to lower frequency in 90% glycerol/buffer solution. The photoproduct spectra for the imidazole and 4-methyl imidazole adducts show shifts of 0 and +1 cm^{-1} in 90% glycerol. These shifts result in a *CO-deoxy difference frequency that is both positive in value and larger for the H93G(Im) and H93G(4-MeIm) adducts in 90% glycerol/buffer solution than in buffer alone, and is consistent with the data obtained for wild-type Mb.

The deoxy H93G(2-MeIm) species shows an increase of 2 cm^{-1} in the ν(Fe–His) frequency in 90% glycerol, while the photoproduct of this species shows a decrease of 1 cm^{-1}. Both of these values are in the opposite direction of what is normally seen for wild-type Mb in 90% glycerol, and thus the *CO-deoxy difference frequency is decreased to 8 cm^{-1}, a value significantly smaller value than the 11 cm^{-1} shift seen in buffer. The frequencies of both the H93G(2-MeIm) and H93G(4-MeIm) differ from those reported in the previous study that used continuous wave laser excitation [36]. The origin of these differences is not known at present and may result from laser excitation using 8 ns pulses. Following photolysis of CO, some imidazole proximal ligands in H93G dissociate on a time scale much longer than 8 ns. This is certainly the case for H93G-*CO shown in Fig. 3, as it is known that a ligand switch occurs in H93G-*CO [32]. Of the ligands used in this study, it is likely that 2-methyl imidazole dissociates the most rapidly given the steric hindrance between the 2-methyl group of this ligand and the heme.

Unlike the other ligands, H93G(1-MeIm)*CO shows no shift in the photoproduct spectrum obtained in 90% glycerol/buffer or in buffer alone. The relative intensities of the two bands in the Fermi doublet change as the protein relaxes from the photoproduct intermediate conformation to the deoxy state in buffer while in 90% glycerol/buffer solvent less difference in relaxation is seen. In 90% glycerol the photoproduct peaks are essentially the same as in buffer, while the deoxy peaks change intensity such that they more closely resemble the photoproduct spectra.

Figure 3 shows the spectra obtained for the H93G protein prepared without exogenous ligand, denoted the

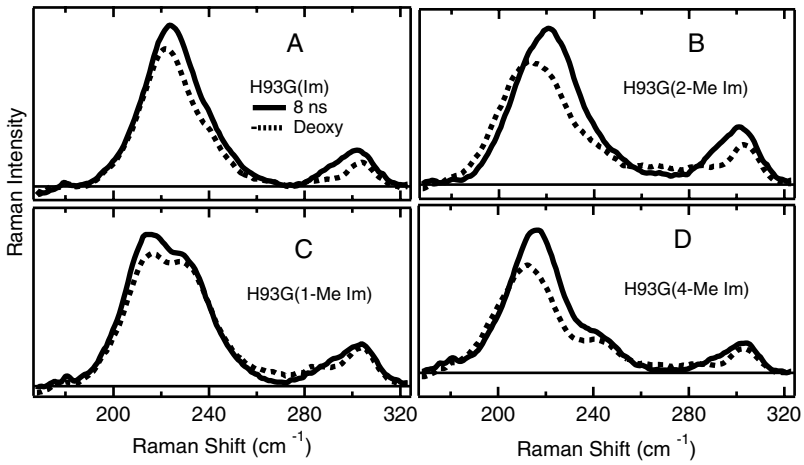

Fig. 2. Equilibrium deoxy and 8 ns photoproduct resonance Raman spectra for H93G(L) Mb with exogenous ligands in 90% glycerol/buffer solution. (A) L = imidazole; (B) L = 2-MeIm; (C) L = 1-MeIm; and (D) L = 4-MeIm. The feature at 180 cm^{-1} is artifact from the hydrogen Raman shifter used in the experiment. The mode at ≈300 cm^{-1} is γ_7 [35].

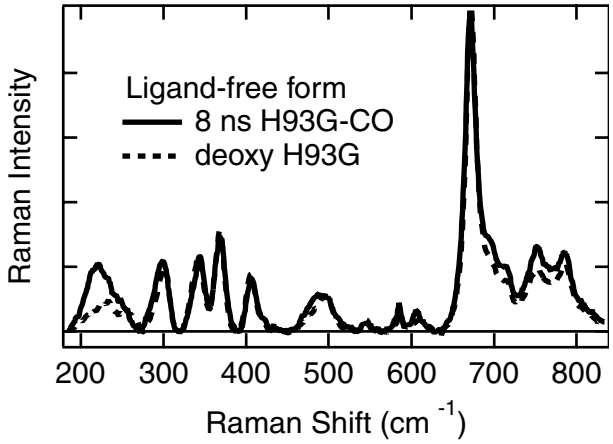

Fig. 3. Equilibrium deoxy and 8 ns photoproduct resonance Raman spectra for H93G-CO Mb with no exogenous ligand. The sample was prepared by heme reconstitution into apoMb in 10 mM phosphate buffer [32]. The dashed line is the deoxy H93G sample and the solid line is the 8 ns photoproduct spectrum.

ligand-free form of H93G. Earlier work shows that the ground state spectrum of the exogenous ligand-free form with CO bound (H93G-CO) has Fe–C and CO stretching frequencies similar to wild-type Mb determined by resonance Raman and FTIR spectroscopy, respectively [32]. The nomenclature H93G-CO reflects the fact that no exogenous proximal ligand is added during sample preparation. However, the exogenous ligand-free adduct of deoxy H93G has a five-coordinate heme high frequency Raman spectrum (spin sensitive region, 1300–1650 cm^{-1}), in spite of the fact that there is no evidence of an axial ligand in the spectral region from 200 to 250 cm^{-1}. The ν(Fe–L) axial iron–ligand out-of-plane mode is absent in the H93G Raman spectrum. The small bands observed at 240 cm^{-1} in the H93G spectrum shown in Fig. 3 are present in all heme resonance Raman spectra of Mb and have been assigned to the A_{1g} mode ν_9 [35]. The 8 ns photoproduct spectrum shown in Fig. 3 reveals the appearance of a ν(Fe–L) band in H93G-*CO. The photoproduct spectra obtained for H93G(Im), H93G(1-MeIm), H93G(2-MeIm) and H93G(4-MeIm) serve as a reference for studies of the ligand-free H93G protein. The appearance of a band at 220 cm^{-1} in the photoproduct spectrum of H93G-*CO is similar to the average frequency for the wild-type, H93G(4-MeIm), H93G(2-MeIm) and H93G(Im) photoproduct spectra in buffer indicating the presence of a nitrogenous imidazole ligand in H93G-*CO.

Raman spectra for all samples in this study exhibit essentially identical high frequency modes. For example, the ν_7 band at 672 cm^{-1} in the H93G(Im) adducts studied in buffer and 90% glycerol/buffer show shifts of less than 0.2 cm^{-1}. Similar observations have been made for the electron density marker and core size modes of deoxy and photoproduct spectra in previous studies [32,36].

DISCUSSION

The photoproduct spectra indicate that there are significant differences in the dynamics for heme iron ligands in the proximal cavity during the first 8 ns following CO photolysis. As the proximal ligands are not covalently bound to the protein, the dynamics can arise from three effects. First, steric interactions between the some of the ligands (e.g. 2-methyl imidazole) and the heme may occur during the change of the iron spin state from low spin in H93G(L)CO to high spin in deoxy H93G(L). Second, steric interactions of the protein may cause ligands to reorient following photolysis. For example, the methyl groups of ligands such as 4-methyl imidazole and 1-methyl imidazole may interact with protein side chains and the methyl group of the 2-methyl imidazole interacts strongly with the heme. Third, changes in ligation or ligand switching can occur due to proximal ligand lability, as has been proposed for the H93G*-CO photoproduct [32]. We consider each of these effects in photoproducts of H93G(L)*CO where L is Im, 2-MeIm, 1-MeIm and 4-MeIm. The photoproduct data on H93G*-CO provides further evidence for the model presented in a previous study [32] in which a histidine from the globin is bound in the six-coordinate form of the H93G mutant when no exogenous proximal ligand is present.

The relative thermodynamic stability of the ligands in the proximal pocket has been determined [29]. The increased relative stability of imidazole and 4-methyl imidazole ligands over the 1-methyl and 2-methyl imidazoles is likely due to the fact that the first two species are closest in binding geometry to the wild-type histidine side-chain. It is expected that Im and 4-MeIm would fit the pocket well and are stabilized by hydrogen bonds similar to those in wild-type Mb. However, the X-ray crystal structure for H93G(4-MeIm) indicates an Np–Fe–Nε–Cδ dihedral angle of 49° for H93G(4-MeIm) as opposed to 38° for H93G(Im) (wild type has an ~10° dihedral angle). Moreover, the imidazole plane in H93G(4-MeIm) is tilted away from the heme normal by more than 10°, creating a geometric distortion that leads to a much shorter hydrogen bond to Ser92 [34]. These data are significant because the stability of the ligand in the photoproduct state is key to understanding the Raman band shifts observed here.

Spectral changes reflect strain and coupling of ligand and porphyrin modes: H93G(2-MeIm) models conformational changes in Hb

The change in frequency for the photoproduct spectrum relative to the equilibrium deoxy spectrum of H93G(2-MeIm) is surprisingly similar to that for photolyzed carbonmonoxy Hb (Hb*CO). In Hb*CO, there is good evidence that strain introduced by changes in protein conformation is communicated to the heme iron [33]. The shift of the ν(Fe–His) band from 230 cm^{-1} in Hb*CO to ≈213 cm^{-1} in deoxy Hb provides key evidence for a mechanism that involves the communication of strain introduced at protein subunits to the diatomic binding site at the iron [33,38,39]. This 17 cm^{-1} shift is comparable to the shift observed in the photoproduct H93G(2-MeIm) adduct in buffer solution. Adducts of heme model systems with 2-methyl imidazole have been used a models of the strain in the deoxy state of Hb (T-state) [40]. The data in Fig. 1 suggest that H93G(2-MeIm) may be an excellent example of the effect of strain on the heme iron in a protein model system.

The origin of proximal histidine strain in Hb involves more than simply an increase in the histidine–iron bond

length with a concomitant weakening of the bond. Models of strain in human Hb also include the tilting of the imidazole due to translation of the F-helix as it makes contact with the CD loop region of a neighboring subunit resulting in the formation of salt bridges and hydrophobic contacts [41]. Changes in the iron–ligand bond tilt angle may modify the ν(Fe–L) stretching frequency through anharmonic coupling to low frequency modes [42]. In analogy with Hb, the large shift in photoproduct ν(Fe–L) frequencies for H93G(2-MeIm)*CO observed in both buffer and 90% glycerol/buffer (Figs 1 and 2, respectively) strongly suggests that proximal strain is present in H93G(2-MeIm)*CO and that this strain arises from a time-dependent change in Np–Fe–Nε tilt angle as the 2-MeIm ligand relaxes in the proximal pocket.

In wild-type Mb*CO the protein relaxations are smaller than in Hb*CO. The frequency shift of the ν(Fe–His) band for the Mb photoproduct (1.5 cm^{-1}) following photolysis is very small compared to that for the Hb photoproduct (12–17 cm^{-1}). Figure 1 shows that the frequency shifts for H93G(Im)*CO and H93G(4-MeIm)*CO photoproduct spectra are similar in magnitude (i.e. very small) to those observed in Mb*CO, however, their sign is reversed. The changes in Mb structure upon photolysis can be divided conceptually into a distal and proximal component [43]. On the distal side, the protein structure must accommodate the photolyzed ligand in a docking site parallel to the heme plane. On the proximal side, the structural changes in both Hb and Mb must also allow the heme iron to move out of the heme plane as it changes from low spin to high spin following photolysis and in Hb this movement is ultimately followed by a shifting of the F-helix. These changes in protein conformation in the proximal cavity of the H93G mutants can have an effect on the stability and electronic structure of the bound proximal ligand and thereby are also reflected in spectroscopic changes in ν(Fe–L) that are sensitive to the heme pocket conformation.

The significance of Soret band shift, ν(Fe–L) shifts and geminate recombination rates

In an earlier study, time-dependent frequency shifts of the heme deoxy Soret band following photolysis in 90% glycerol/buffer solution were observed for the species H93G(Im)CO, H93G(4-MeIm)CO, and H93G(1-MeIm)-CO as well as wild-type Mb [44]. For these proximal ligands, the time scale of the Soret band shift at room temperature was nearly identical ($< 10^{-6}$ s), although there was a slight increase in the rate in the order wild type < 1-methyl imidazole ≅ 4-methyl imidazole < imidazole. For this same set of proximal ligands, the geminate phase of the CO rebinding was found to increase in the order wild type < 4-methyl imidazole < imidazole < 1-methyl imidazole and occurred on a time scale similar to the Soret band shift [30]. As shown in Table 1, in 90% glycerol the difference in the photoproduct vs. deoxy ν(Fe–L) Raman frequencies, CO–deoxy, for these ligands decreases in the same order that the previously reported geminate rate increased: wild type (4 cm^{-1}) = 4-methyl imidazole (4 cm^{-1}) > imidazole (2 cm^{-1}) > 1-methyl imidazole (0 cm^{-1}). From these data it would appear that the conformational coordinates that control the Soret shift in H93G(L)*CO are not related to those that govern the geminate rebinding rate and the shift in the photoproduct ν(Fe–L) frequency from its equilibrium deoxy position but that the latter two observable phenomena are correlated. These phenomena are consistent with a separation of contributions from proximal and distal pocket conformational relaxations that can be understood as follows. The observed geminate phase decay rate can be expressed as the sum of two rates for a three state model: the rebinding rate for the CO from within the pocket and the escape of the CO to the solvent, $k_{gem} = k_{21} + k_{23}$, where the system can be portrayed as follows:

$$\mathrm{MbCO} \underset{k_{12}}{\longleftrightarrow} \mathrm{Mb{:}CO} \underset{k_{23}}{\longleftrightarrow} \mathrm{Mb} + \mathrm{CO}$$

The rebinding rate, k_{21}, is a function of the rebinding barrier, and this is in part controlled by the strain on the proximal ligand after photolysis as observed in the photoproduct spectra. The difference in the photoproduct ν(Fe–L) frequency with respect to the deoxy value correlates well with the amount of geminate rebinding that occurs and this is interpreted to be due to the fact that the ν(Fe–L) frequency typically decreases due to an increase in proximal strain in the Fe–L bond, as described above. On the other hand, the escape rate, k_{23}, is largely controlled by distal pocket conformational changes. The Soret band shift and the escape rate constant k_{23} are not highly dependent on the identity of the proximal ligand in H93G(L)*CO [30,44]. However, mutations in the distal heme pocket result in changes that are distinct from those of H93G; the Soret band shift, k_{23} and k_{21} are all affected concomitantly [16,47].

H93G(1-MeIm) probes hydrogen bonding in the proximal pocket

The X-ray crystal structure of the metaquo form of H93G(4-MeIm) and H93G(1-MeIm) show nearly identical conformations for methyl imidazole in the proximal pocket [34]. The X-ray structure for H93G(4-MeIm) is consistent with hydrogen bonding for 4-methyl imidazole with S92 that is stronger than in wild-type Mb. However, no hydrogen bonding is possible for 1-methyl imidazole because the Nδ position is bonded to a methyl group in this ligand. Moreover, the p*K*a is similar for both H93G(4-MeIm) and H93G(1-MeIm) indicating that differences in frequency are not due to differences in ligand basicity. Nonetheless, there is a substantial difference in the proximal dynamics for these two ligands. It is reasonable to suggest that the inability of 1-methyl imidazole to form a hydrogen bond is responsible for the differences in proximal dynamics [29]. Comparison with other proximal mutations such as S92A and L89I indicates that hydrogen bonding does not have a large effect when native histidine is ligated to the heme iron [45]. However, proximal ligands are destabilized by the H93G/S92A double mutant so that no ν(Fe–L) frequencies have been obtained for the latter [29]. Thus, hydrogen bonding likely has a larger effect on the non-native ligands to heme iron in H93G(L) and H93G(L)*CO than observed in mutants such as S92A or L89I that remove hydrogen bonds to Nδ-H. For example, neither viscosity/hydration effects from addition of glycerol nor photoproduct spectra affect the frequency of the nonhydrogen-bonding ligand H93G(1-MeIm) shown in Figs 1 and 2.

Ligand-free H93G data indicate a ligand switching mechanism

The covalent attachment of the ligand can be affected by the change in hydrogen bonding suggesting that ligand lability (i.e. a ligand switch) may also be a factor in differences in ν(Fe–L) frequency observed in Figs 1 and 2. Evidence for a ligand switch can be obtained by comparison of the photoproduct spectra with time-resolved FTIR and saturation Raman experiments on H93G-CO. The ligand switch does not appear to occur on an ultrafast time scale. In fact, it appears to be quite slow (> 5 μs) [32]. The six-coordinate form of H93G-CO appears to have a nitrogenous ligand bound to the heme iron as shown in Fig. 3. The photoproduct data provide evidence that the ligand *trans* to CO in H93G-CO is an endogenous histidine and likely is His97.

The ligand-free H93G*-CO photoproduct spectrum shown in Fig. 3 has an interesting effect not observed for the imidazole adducts. The deoxy spectrum shows no axial ν(Fe–L) mode. However, there must be an axial ligand because the high frequency region of the deoxy spectrum is consistent with a five-coordinate heme adduct. The buffer contains only 10 mM phosphate and thus the axial ligand in H93G must be H_2O, phosphate or an amino acid side chain. The photoproduct spectrum shows a distinct increase in intensity at 220 cm^{-1} consistent with a change in ligation. In a previous study we proposed that the axial ligand is H_2O in H93G, i.e. H93G(H_2O), and a histidine residue in H93G*-CO [i.e. H93G(His)CO]. Most likely, the axial ligand observed in the CO photoproduct spectrum is also bound *trans* to CO in the equilibrium form of H93G-CO. This ligand is hypothesized to be a histidine due to the frequency of 220 cm^{-1}, which is almost identical to that of wild-type Mb. Although assignment of the histidine is not certain, studies of the CO stretching frequency for double mutants indicate that the distal histidine (His64) probably does not give rise to the signal observed in Fig. 3 [46]. His97 is immediately adjacent to His93 on the proximal side and we are currently investigating whether it is the side chain that ligates the heme iron *trans* to CO in H93G-CO.

The data in Fig. 3 indicate that the axial ligand of the heme iron is not the same in the H93G-CO and deoxy H93G species. This is in agreement with step-scan FTIR and saturation Raman data that indicate a dynamic ligand switch in H93G Mb [32]. The histidine that appears bound in the 8 ns photoproduct spectrum dissociates from the iron on a time scale < 5 μs. CO recombines to give rise to a transient H93G(H_2O)CO species. This species then returns to the equilibrium form, H93G(His)CO, on the millisecond time scale. If His97 is ligated to the heme iron, it must be sufficiently unstable that it is replaced by H_2O in the deoxy form. Substantial protein strain is required to permit His97 ligation. Furthermore, it is nearly impossible for His97 to hydrogen bond in a manner analogous to His93. Thus, the dynamic change in ligation is driven by conformational strain the H93G(His)CO protein.

CONCLUSION

The 8 ns CO photoproduct spectra of the ν(Fe–L) band in H93G Mb reveal an important role for steric interactions and hydrogen bonding in the proximal pocket. The shifts in the ν(Fe–L) photoproduct spectra of H93G(Im)*CO, H93G(4-MeIm)*CO and H93G(1-MeIm)*CO are small or absent, while the shift is relatively large for H93G(2-MeIm). The Raman data further confirm the hypothesis that the ligand-free form is a H93G(His)CO adduct that is strained. In this adduct, the histidine dissociates within 5 μs after CO photolysis but is clearly bound 8 ns after photolysis as shown in Fig. 3. There is no evidence for a four-coordinate intermediate in heme dissociations of this type and it is likely that the off-rate of the ligand is slow because of the requirement for water to enter the proximal cavity to serve as a replacement for the nitrogenous ligand. Thus, the proximal ligand in H93G(L)*CO is destabilized leading to dissociation or altered frequencies due to ligand strain. The stability of the proximal ligand is also modulated by the strength of Nδ-H hydrogen bond.

Although the relaxation in the proximal pocket shown here does not affect the distal pocket relaxation probed by the Soret band shift or band III shift, it may affect CO rebinding kinetics [44]. For example, although H93G(1-MeIm) and H93G(4-MeIm) are isostructural and have similar basicity, their CO rebinding kinetics are quite different [30]. H93G(1-MeIm) has a geminate recombination rate constant nearly one order of magnitude larger than that of H93G(4-MeIm) in a 90% glycerol/buffer glass [44]. Both ligand strain and proximal ligand dissociation can lead to rapid CO rebinding kinetics. Thus, the ligands that cannot hydrogen bond and fit poorly in the proximal pocket are expected to have more rapid geminate CO recombination rate constants. The data presented here show the utility of the H93G mutant for separating proximal and distal effects in Mb. This is a key step toward making definitive assignments of spectroscopic shifts in terms of globin structure. The ν(Fe–L) band shifts measured in this study further support the model advanced earlier that protein relaxation monitored by band III and the Soret band shifts represents motions of amino acid residues in the distal pocket in response to CO photolysis. The distal relaxation is distinct from the proximal effects observed here that previously have been demonstrated to have a large effect on the kinetics of geminate CO recombination.

ACKNOWLEDGMENTS

SF acknowledges support by the NSF (MCB–9874895); JMF acknowledges support from NIH (R01 HL58247, RO1 G58890) and the W.M. Keck Foundation; and SGB acknowledges support from NIH (GM27738).

REFERENCES

1. Rousseau, D.L. & Friedman, J.M. (1988) In: *Biological Applications of Raman Spectroscopy*, Vol. III (Spiro, T.G., ed), pp. 133–215. Wiley & Sons, New York.
2. Kitagawa, T. (1988) Biological applications of raman spectroscopy. In *Biological Applications of Raman Spectroscopy*, Vol. III (Spiro, T.G., ed), pp. 97–131. Wiley & Sons, New York.
3. Jayaraman, V., Rodgers, K.R., Mukerji, I. & Spiro, T.G. (1995) Hemoglobin allostery: resonance Raman spectroscopy of kinetic intermediates. *Science* **269**, 1843–1848.
4. Barrick, D. (2000) Trans-substitution of the proximal hydrogen bond in myoglobin. II. Energetics, functional consequences, and implications for hemoglobin allostery. *Proteins Struct. Func. Genet.* **39**, 291–308.

5. Scott, T.W. & Friedman, J.M. (1984) Tertiary-structure relaxation in hemoglobin: a transient Raman study. *J. Am. Chem. Soc.* **106**, 5677–5687.
6. Petersen, E., Chien, E., Sligar, S. & Friedman, J. (1998) Functional implications of the proximal hydrogen-bonding network in myoglobin. A resonance Raman and kinetic study of Leu89, Ser92, His97 and F-helix swap mutants. *Biochemistry* **37**, 12301–12319.
7. Jackson, T.A., Lim, M. & Anfinrud, P.A. (1994) Complex non-exponential relaxation in myoglobin after photodissociation of MbCO: measurement and analysis from 2 ps to 56 μs. *Chem. Phys.* **180**, 131–140.
8. Gilch, H., Schweitzer-Stenner, R., Dreybrodt, W., Leone, M., Cupane, A. & Cordone, L. (1996) Conformational substates of the Fe^{2+}–His F8 linkage in deoxymyoglobin and hemoglobin probed in parallel by the Raman band of the Fe–His stretching vibration and the near infrared absorption band III. *Int. J. Quantum Chem.* **59**, 301–313.
9. Chavez, M.D., Courtney, S.H., Chance, M.R., Kuila, D., Nocek, J., Hoffman, B.M., Friedman, J.M. & Ondrias, M.R. (1990) Structural and functional significance of inhomogeneous line broadening of band III in hemoglobin and Fe–Mn hybrid hemoglobins. *Biochemistry* **29**, 4844–4852.
10. Kiger, L., Stetzkowski-Marden, F., Poyart, C. & Marden, M. (1995) Correlation of carbon monoxide association rates and position of absorption band III in hemeproteins. *Eur. J. Biochem.* **228**, 665–668.
11. Schlichting, I., Berendzen, J., Phillips, G.N. Jr & Sweet, R.M. (1994) Crystal structure of an intermediate of CO binding to myoglobin. *Nature* **371**, 808–812.
12. Srajer, V., Teng, T.Y., Ursby, T., Pradervand, C., Ren, Z., Adachi, S., Schildkamp, W., Bourgeois, D., Wulff, M. & Moffat, K. (1996) Photolysis of the carbon monoxide complex of myoglobin: nanosecond time resolved crystallography. *Science* **274**, 1726–1729.
13. Teng, T.-Y., Srajer, V. & Moffat, K. (1994) Photolysis-induced structural changes in single crystals of carbonmonoxy myoglobin at 40 K. *Nat. Struct. Biol.* **1**, 701–705.
14. Hartmann, H., Zinser, S., Komninos, P., Schneider, R.T., Nienhaus, G.U. & Parak, F. (1996) X-ray structure determination of a metastable state of carbonmonoxy myoglobin after photodissociation. *Proc. Natl Acad. Sci. U.S.A.* **93**, 7013–7016.
15. Lim, M.H., Jackson, T.A. & Anfinrud, P.A. (1997) Ultrafast rotation and trapping of carbon monoxide dissociated from myoglobin. *Nat. Struct. Biol.* **4**, 209–214.
16. Lambright, D.G., Balasubramanian, S. & Boxer, S.G. (1993) Dynamics of protein relaxation in site-specific mutants of human myoglobin. *Biochemistry* **32**, 10116–10124.
17. Ansari, A., Jones, C.M., Henry, E.R., Hofrichter, J. & Eaton, W.A. (1992) Conformational relaxation and ligand rebinding in myoglobin. *Science* **256**, 1796–1798.
18. Steinbach, P.J., Ansari, A., Berendzen, J., Braunstein, D., Chu, K., Cowen, B.R., Ehrenstein, D., Frauenfelder, H., Johnson, J.B., Lamb, D.C., Luck, S., Mourant, J.R., Nienhaus, G.U., Ormos, P., Philipp, R., Xie, A. & Young, R.D. (1991) Ligand binding to heme proteins: connection between dynamics and function. *Biochemistry* **30**, 3988–4001.
19. Tian, W.D., Sage, J.T., Champion, P.M., Chien, E. & Sligar, S.G. (1996) Probing heme protein conformational equilibration rates with kinetic selection. *Biochemistry* **35**, 3487–3502.
20. Ostermann, A., Waschipky, R., Parak, F.G. & Nienhaus, G.U. (2000) Ligand binding and conformational motions in myoglobin. *Nature* **404**, 205–208.
21. Goodin, D.B. & McRee, D.E. (1993) The Asp-His-Fe triad of cytochrome c peroxidase controls the reduction potential, electronic structure, and coupling of the tryptophan free radical to the heme. *Biochemistry* **32**, 3313–3324.
22. Smulevich, G., Hu, S.Z., Rodgers, K.R., Goodin, D.B., Smith, K.M. & Spiro, T.G. (1996) Heme-protein interactions in cytochrome *c* peroxidase revealed by site-directed mutagenesis and resonance Raman spectra of isotopically labeled hemes. *Biospectroscopy* **2**, 365–376.
23. Sun, J., Fitzgerald, M.M., Goodin, D.B. & Loehr, T.M. (1997) Solution and crystal structures of the H175G mutant of cytochrome *c* peroxidase: a resonance Raman study. *J. Am. Chem. Soc.* **119**, 2064–2065.
24. Vogel, K.M., Spiro, T.G., Shelver, D., Thorsteinsson, M.V. & Roberts, G.P. (1999) Resonance Raman evidence for a novel charge relay activation mechanism of the CO-dependent heme protein transcription factor CooA. *Biochemistry* **38**, 2679–2687.
25. Callahan, P.M. & Babcock, G.T. (1981) Insights into heme structure from soret excitation Raman spectroscopy. *Biochemistry* **20**, 952–958.
26. Schelvis, J.P.M., Kim, S.Y., Zhao, Y.D., Marletta, M.A. & Babcock, G.T. (1999) Structural dynamics in the guanylate cyclase heme pocket after CO photolysis. *J. Am. Chem. Soc.* **121**, 7397–7400.
27. Frauenfelder, H., McMahon, B.H., Austin, R.H., Chu, K. & Groves, J.T. (2001) The role of structure, energy landscape, dynamics, and allostery in the enzymatic function of myoglobin. *Proc. Natl Acad. Sci. USA* **98**, 2370–2374.
28. Kuriyan, J., Wilz, S., Karplus, M. & Petsko, G.A. (1986) *J. Mol. Biol.* **192**, 133–154.
29. Decatur, S.M., Belcher, K.L., Rickert, P.K., Franzen, S. & Boxer, S.G. (1999) Hydrogen bonding modulates binding of exogenous ligands in a myoglobin proximal cavity mutant. *Biochemistry* **38**, 11086–11092.
30. Franzen, S. (2002) Carbonmonoxy rebinding kinetics in h93g myoglobin: separation of proximal and distal side effects. *J. Phys. Chem.* **106**, 4533–4542.
31. DePillis, G., Decatur, S.M., Barrick, D. & Boxer, S.G. (1994) Functional cavities in proteins – a general method for proximal ligand subsitution in myoglobin. *J. Am. Chem. Soc.* **116**, 6981–6982.
32. Franzen, S., Bailey, J., Dyer, R.B., Woodruff, W.H., Hu, R.B., Thomas, M.R. & Boxer, S.G. (2001) A photolysis-triggered heme ligand switch in H93G myoglobin. *Biochemistry* **40**, 5299–5305.
33. Petersen, E.S. & Friedman, J.M. (1998) A possible allosteric communication pathway identified through a resonance Raman study of four beta 37 mutants of human hemoglobin A. *Biochemistry* **37**, 4346–4357.
34. Barrick, D. & Dahlquist, F.W. (2000) Trans-substitution of the proximal hydrogen bond in myoglobin. I. Structural consequences of hydrogen bond deletion. *Proteins Struct. Func. Genet.* **39**, 278–290.
35. Hu, S., Smith, K.M. & Spiro, T.G. (1996) Assignment of protoheme resonance Raman spectrum by heme labeling in myoglobin. *J. Am. Chem. Soc.* **118**, 12638–12646.
37. Sage, J.T., Schomacker, K.T. & Champion, P.M. (1995) Solvent-dependent structure and dynamics in myoglobin. *J. Phys. Chem.* **99**, 3394–3405.
36. Franzen, S., Boxer, S.G., Dyer, R.B. & Woodruff, W.H. (2000) Resonance Raman studies of heme-axial ligation in H93G myoglobin. *J. Phys. Chem. B* **104**, 10359–10367.
38. Matsukawa, S., Mawatari, K., Yoneyama, Y. & Kitagawa, T. (1985) Correlation between the iron-histidine stretching frequencies and oxygen affinity of hemoglobins. A continuous strain model. *J. Am. Chem. Soc.* **107**, 1108–1113.
39. Friedman, J.M., Scott, T.W., Stepnowski, R.A., Ikeda-Saito, M. & Yonetani, T. (1983) The iron-proximal histidine linkage and protein control of oxygen binding in hemoglobin. *J. Biol. Chem.* **258**, 10564–10572.
40. Nagai, K., Kitagawa, T. & Morimoto, H. (1980) Quaternary structures and low frequency molecular vibrations of haems of

deoxy and oxyhaemoglobin studied by resonance Raman scattering. *J. Mol. Biol.* **136**, 271–289.
41. Franzen, S., Lambry, J.C., Bohn, B., Poyart, C. & Martin, J.L. (1994) Direct evidence for heme-iron doming as the primary event in the quaternary structure change of hemoglobin. *Nat. Struct. Biol.* **1**, 230–233.
42. Rosenfeld, Y.B. & Stavrov, S.S. (1994) Anharmonic coupling of soft modes and its influence on the shape of the iron-histidine resonance Raman band of heme proteins. *Chem. Phys. Lett.* **229**, 457–464.
43. Franzen, S., Bohn, B., Poyart, C. & Martin, J.L. (1995) Evidence for sub-picosecond heme doming in hemoglobin and myoglobin. A time-resolved resonance Raman comparison of carbonmonoxy and deoxy species. *Biochemistry* **34**, 1224–1237.
44. Franzen, S. & Boxer, S.G. (1997) On the origin of heme absorption band shifts and associated protein structural relaxation in myoglobin following flash photolysis. *J. Biol. Chem.* **272**, 9655–9660.
45. Peterson, E., Chien, E., Sligar, S. & Friedman, J. (1998) Functional implications of the proximal hydrogen-bonding network in myoglobin. A resonance Raman and kinetic study of Leu89, Ser92, His97 and F-helix swap mutants. *Biochemistry* **37**, 12301–12319.
46. Hu, R.B. (1999) *Structure-Function Relationship in Myoglobins with Distal and Proximal Mutation*, PhD Thesis, Stanford University, Stanford, CA, USA.
47. Nienhaus, K., Lamb, D.C., Deng, P. & Nienhaus, G.U. (2002) The effect of ligand dynamics on heme electron transition band III in myoglobin. *Biophys. J.* **82**, 1059–1067.